Available online at www.sciencedirect.com
ScienceDirect
Catalysis Today 127 (2007) 337–346
CATALYSIS TODAY
www.elsevier.com/locate/cattod

Study of the reverse water gas shift (RWGS) reaction over Pt in a solid oxide fuel cell (SOFC) operating under open and closed-circuit conditions

G. Pekridis [a], K. Kalimeri [a], N. Kaklidis [a], E. Vakouftsi [a], E.F. Iliopoulou [b], C. Athanasiou [a,c], G.E. Marnellos [a,b,*]

[a] Department of Engineering and Management of Energy Resources, University of Western Macedonia, Bakola & Sialvera, GR-50100 Kozani, Greece
[b] Chemical Process Engineering Research Institute, Centre for Research & Technology Hellas, 6th km Charilaou, Thermi Road, P.O. Box 361, GR-57001 Thermi, Thessaloniki, Greece
[c] Department of Chemical Engineering, Aristotle University of Thessaloniki, University Campus, P.O. Box 1517, GR-54006 Thessaloniki, Greece

Available online 2 July 2007

Abstract

The (electro-)kinetics of the reverse water gas shift (RWGS) reaction was studied in a solid oxide fuel cell (SOFC) of the type Pt/YSZ/Pt. The effect of imposed potentials, cell temperature (650–800 °C), H_2 (1–10 kPa) and CO_2 (1–10 kPa) partial pressures on the kinetics and mechanism of the catalytic and electrocatalytic RWGS reaction, were systematically examined. The apparent catalytic activation energy was found equal to 15.6 kcal/mol, while H_2 and CO_2 apparent reaction orders were equal to 0.5 and 0.7, respectively. At both open and closed circuit operation, the associative formate decomposition reaction mechanism was considered to describe kinetics. Under closed circuit operation, rate enhancement factor, $|\Lambda|$, values up to 10 were achieved. Finally, current density–voltage and current density–power density characteristics of the cell were recorded at various temperatures and gas mixtures of CO_2 and H_2. It was found that electrical power output of the cell was optimized by increasing temperature and decreasing CO_2/H_2 feed ratio. Maximum power density obtained was 9 mW/cm^2 (at 520 mV cell voltage and a current density of 17.3 mA/cm^2, at 800 °C and $P_{CO_2}/P_{H_2} = 0.16$).

Keywords: Reverse water gas shift; Solid oxide fuel cell; Platinum; Yttria stabilized zirconia; Non-Faradaic electrochemical modification of catalytic activity; Electrochemical promotion

1. Introduction

Water–gas shift (WGS) reaction is a key step process in many industrial applications such as production of fuels and useful chemicals [1]:

$$CO + H_2O \leftrightarrow CO_2 + H_2, \quad \Delta H^\circ_{rxn} = -41.2\,kJ/mol, \quad \Delta G^\circ_{rxn} = -28.6\,kJ/mol \tag{1}$$

WGS is a very fast reaction, which easily reaches equilibrium. Therefore, both forward and reverse water–gas shift (RWGS) reactions take place in the converter and, depending on the reaction conditions, equilibrium is shifted to the right or to the left. Both reactions are involved in the production of syngas, where they are mostly used in combination with partial oxidation and reforming of hydrocarbons in order to fix the H_2/CO ratio. This adjustment is very important, since different industrial applications (e.g. methanol and ammonia synthesis, Fischer-Tropsch synthesis and fuel processing for fuel cells) require different H_2/CO ratios [1,2]. Specifically, RWGS reaction technology is expected in many industries in the production of useful CO from cheap CO_2, since CO is valuable and necessary in many chemical companies [3].

Although fuel cells operate efficiently on H_2, there are still some major problems related to hydrogen availability and acceptability. Consequently, in order to accelerate fuel cells' commercialization research must be directed towards the development of fuel cells able to operate with fuels other than hydrogen, such as commercial (e.g. natural gas, LPG, gasoline and diesel) or ''green'' fuels (bio-fuels) [4]. On the other hand,

* Corresponding author at: Department of Engineering and Management of Energy Resources, University of Western Macedonia, Bakola & Sialvera, GR-50100 Kozani, Greece. Tel.: +30 2461 0 56690; fax: +30 2461 0 56601.
E-mail addresses: marnel@cperi.certh.gr, gmarnellos@uowm.gr (G.E. Marnellos).

0920-5861/$ – see front matter © 2007 Elsevier B.V. All rights reserved.
doi:10.1016/j.cattod.2007.05.026

the conjunction of solid oxide fuel cells (SOFCs) with biomass gasification or other thermochemical conversion methods can be a highly efficient, promising technology toward the production of ''green'' power [5]. Biomass gasification produces gas mixtures of bio-fuels, that consist mainly of H_2 (20–25%), CO (25–30%) and CO_2 (10–15%) [6]. Therefore, via RWGS reaction, it is possible to adjust the CO/H_2 ratio by converting the inert CO_2 to fuel CO and decreasing at the same time, the H_2 content in the gas mixture. This shift in fuels composition is dictated by thermodynamics, since CO combustion enthalpy change is slightly higher compared to the corresponding enthalpy change of H_2, thus achieving higher electrical efficiencies in fuel cells. In addition, concerning kinetics, CO is oxidized much faster than H_2 over a variety of anodic electrodes-catalysts, especially over Pt-based electrocatalysts [7].

Moreover, utilization of CO_2 has become an important global issue due to the significant and continuous rise in atmospheric CO_2 concentrations [8]. Conversion of CO_2 to CO by catalytic reactions has been widely recognized as one of the most promising processes for CO_2 utilization [8]. Using RWGS reaction, CO_2 is converted to CO and simultaneously, if the whole process is going to take place in a fuel cell, to the generation of electrical energy.

Up to date, two main reaction mechanisms have been proposed for the catalytic WGS and RWGS reaction [9]. However it is not yet completely clear, which of them is the prevailing one [10]. According to the first, the ''redox'' mechanism, CO is adsorbed on reduced metal sites and reacts with an oxygen atom coming from the support to CO_2. In the following, the reduced support is subsequently re-oxidized by water, releasing hydrogen [11–15]. In the second, the associative ''formate'' mechanism, the main reaction intermediate is a bi-dentate formate, produced by the reaction of CO with terminal hydroxyl groups on the oxide support, which decomposes to form H_2 and a mono-dentate carbonate [16–22]. RWGS reaction is readily catalyzed by both noble (e.g. Pt, Ru, Pd) and transition (e.g. Cu, Ni, Fe, Co) metals supported over various metal oxides (e.g. γ-Al_2O_3, CeO_2, SiO_2). However, the majority of the studies refer to Cu and Pt catalysts. Prichard and Hinshelwood studied the kinetics of the RWGS reaction over platinum in 1925 [23]. Amenomiya investigated the kinetics of both WGS and RWGS reactions and identified the presence of formate intermediate in both reactions [24,25]. Depending on the direction of the WGS reaction, this formate intermediate was decomposed into either CO_2 and H_2 or CO and H_2O. However, although Cu-based catalysts have been widely used in WGS-RWGS applications [3,26–29], Cu exhibits a pyrophoric nature and deactivates in the presence of air and condensed water [27]. Recently, emphasis was given to the platinum-based catalysts. The effect of carbon deposition in the deactivation of a 2% Pt/CeO_2 under RWGS reaction conditions has been investigated in depth [30], and it was found that exposure to CO led to severe deactivation, while exposure to CO_2, CH_4, or H_2 led to moderate or no deactivation.

Solid state electrochemical cells were first used in 1975 to improve the performance of heterogeneous catalysts [31,32]. Progress in the specific research area was driven to a considerable degree by the work of Vayenas et al. [33], who focused on the *electrochemical promotion* (EP) of catalysts. RWGS reaction has been studied in both oxygen-ion (yttrium stabilized zirconia, YSZ) [34] and proton (yttrium doped strontium zirconate perovskite of the type $SrZr_{0.9}Y_{0.1}O_{3-a}$, where a is the number of oxygen deficiencies per unit cell) [35] conductive solid electrolyte membrane reactors. Over Rh electrodes [34], where the main products were CH_4 and CO, it was found that methane formation was enhanced by applying positive potentials, while on the contrary CO formation was promoted in the case of negative potentials. The phenomenon was non-Faradaic, since reaction rate was enhanced approximately 220 times compared to the rate of the electrochemical supply or removal of oxygen anions [34]. However, when using Pd instead of Rh, only CO was produced and CO_2 was not adsorbed dissociatively. This difference was also reflected in the behaviour of the system since CO formation was enhanced (by up to 600%) not only with decreasing catalyst potential, but also to a minor extent with increasing the catalyst potential [34]. Karagiannakis et al. studied the RWGS reaction in a proton conducting cell [35]. Copper was used as catalyst/electrode. It was found that when hydrogen was supplied electrochemically, the reaction rate was two to five times higher than when only gaseous hydrogen was fed to the reactor [35].

In the present work, the (electro-)kinetics of the RWGS reaction, carried out in a SOFC of the Pt/YSZ/Pt type, was examined. The effect of imposed potentials, cell temperature, H_2 and CO_2 partial pressures on the kinetics and mechanism of RWGS reaction, was thoroughly studied. Finally, the potential role of the RWGS reaction in the production of electrical power by measuring the voltage–current density and power density–current density characteristics of the ''RWGS'' SOFC at various temperatures and CO_2/H_2 ratios, was investigated.

2. Experimental

2.1. Experimental apparatus

The apparatus used for the (electro)-catalytic measurements consisted of the feeding unit, the cell-reactor and the analysis system. Reactant gases included CO_2/He mixtures, H_2 and He of 99.999% purity, and were supplied by Air Liquide. Reactants and products analysis was performed by using an on-line, SHIMADJU 14B, gas chromatography, equipped with a thermal conductivity detector (TCD). A molecular sieve 13× column (10 ft × 1/8 in.) was used to separate hydrogen and carbon monoxide, while a Porapack QS column (10 ft × 1/8 in.) was employed for the carbon dioxide separation. Both columns were heated at 60 °C. Water concentration was always calculated by applying hydrogen and oxygen mass balances. Moreover, an AMEL model 2053 galvanostat–potentiostat and two differential voltmeters (Digital Multimeter DT9205A) were used to impose potentials (potentiostatic mode of operation) and to measure the developed currents and power densities of the solid oxide fuel cell. It must be noticed here that all potentials are referred to potentials as measured and not to

ohmic-free potentials, where ohmic resistance has been previously subtracted.

Platinum working electrode, which also served as the catalyst of the RWGS reaction, was prepared from a platinum paste (Engelhard A1121), and deposited on the inside bottom of the YSZ tube, resulting in an apparent surface area of 2.5 cm^2. The catalyst loading was approximately 250 mg. Scanning electron microscopy examination of the catalyst showed an average particle size of the crystallites of about 0.4 μm. Using the catalyst loading and the average particle size of the Pt crystallites, a catalytic surface area of approximately 1810 cm^2, was calculated. Platinum paste was also used for the preparation of the counter (apparent surface area equal to 2 cm^2) and reference (apparent surface area equal to 0.2 cm^2) electrodes. All electrodes were calcined at 800 °C for 0.5 h under stagnant atmospheric air before use (heating rate: 10 °C/min). The electrochemical reactor used in our experiments is described in detail in previous communications [36] and consisted of a YSZ tube (19 mm O.D., 16 mm I.D., 15 cm long), closed flat at one end. The open end of the YSZ tube was clamped to a stainless-steel cap, which had provisions for inlet and outlet gas lines. A silver wire was used to establish electrical contact with the inner platinum catalyst–electrode via a spirally shaped end. The electrical circuit was closed by two others silver wires connected to counter and reference electrodes, respectively. In all cases, the temperature was monitored by a K-type thermocouple, inserted into the furnace, where the reactor was located.

2.2. Experimental procedure

The RWGS reaction was carried out in the continuous flow reactor cell described in the previous section, using various reacting mixtures of CO_2 (1–10%) and H_2 (1–10%) diluted in He, at temperatures between 650 and 800 °C. The electrochemical promotion technique was implemented by applying positive and negative potentials varying from −2000 to 2000 mV, to all reacting gas mixtures. Fuel cell measurements were performed potentiostatically by measuring the developed current and power densities (power per unit area of the apparent electrode surface) between the working and counter electrodes, for each imposed voltage ranging from the open circuit potential (electromotive force of the cell) up to 0 mV. Finally, in all experiments a total volumetric flow rate of 20 cm^3/min STP was fed to the anode, while both counter and reference electrodes were exposed to the ambient atmosphere.

3. Results and discussion

3.1. (Electro-)kinetics of the RWGS reaction

The (electro-)kinetics of the RWGS reaction was thoroughly examined in the Pt/YSZ/Pt oxygen-ion conductive solid electrolyte cell reactor. Fig. 1 shows the effect of temperature (650–800 °C) on the CO formation rate under both open (applied potential: 0 mV) and closed (applied potential: −1000 and 400 mV) circuit operation by using a stoichiometric

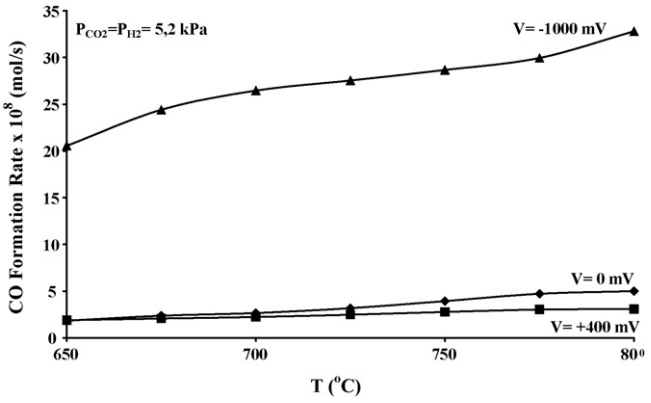

Fig. 1. Effect of cell temperature on CO formation rate under open (0 mV) and closed (−1000 mV and 400 mV) circuit operation. T = 650–800 °C, $P_{H_2} = P_{CO_2}$ = 5.2 kPa, F_T = 20 cm^3/min.

reactants' ratio ($P_{CO_2} = P_{H_2} = 5.2$ kPa). It must be noticed here that YSZ is a purely oxygen conductor and when anodic potentials or currents are imposed, an equivalent to Faradaic law ($I/2F$, where F is Faraday's constant) rate of electrochemical oxygen anions, O^{2-}, are migrating from cathode to anode through the YSZ membrane wall. In the case of cathodic potentials or currents, oxygen anions are removed from the reacting mixture to the cathodic electrode, which is exposed to atmospheric air.

It is clear that both under open and closed circuit operation, CO formation rate increases with increasing temperature. This behaviour is more pronounced in the case of negative potentials. At negative potentials (electrochemical removal of oxygen anions from the reactor cell), CO formation rate was dramatically enhanced, while by supplying oxygen anions electrochemically to the reactor chamber the rate was slightly decreased. A 10-fold increase in CO formation rate was observed at 650 °C in the case of negative voltages (V = −1000 mV, I = −57.2 mA). As the cell temperature was increased, the absolute difference between the closed (both for positive and negative potentials) and open circuit reaction rates, was also increased, while the corresponding ratio of the rates was reduced. On the contrary, water formation (not shown here) was enhanced at positive potentials due to the increased oxygen ion-pumping rate at higher temperatures, resulting in the enhanced electrochemical oxidation of hydrogen. On the other case of imposing negative potentials, water formation was reduced due to the decreased oxygen partial pressure at the anode interface. It must be pointed out here that at voltages higher than 400 mV, CO formation rate was annihilated and therefore only water production rate was increased.

The apparent activation energy of chemical catalytic reaction under open circuit operation was found to be equal to 15.6 kcal/mol. For comparison, activation energy values from 18 to 24 kcal/mol have been reported for the RWGS reaction on metal disulfides [3], transition metal [3], Cu [26] and Cu/ZnO/Al_2O_3 [28] catalysts (Table 1). On the other hand, by supplying or removing electrochemical oxygen the apparent activation energies for the electrocatalytic RWGS reaction are decreased to about 1/3 of the corresponding open circuit value.

Table 1
Reverse water–gas shift (RWGS) reaction kinetic data

Catalyst	Pressure (atm)	Temperature (°C)	P_{CO_2}/P_{H_2}	Activation energy (kcal/mol)	Reaction order		Reference
					CO_2	H_2	
MoS_2	1	300–500	1	18	0.73	0.36	3
WS_2	1	300–500	1	19.1	0.61	0.36	3
Ni/Al_2O_3	1	300–500	1	20.8	0.5	0.81	3
Co/Al_2O_3	1	300–500	1	18.4	0.51	0.59	3
Fe/Al_2O_3	1	300–500	1	18.7	1.1	0.37	3
Cu(1 1 0) Cu(poly)	5.1	200–300	0.1	18.6	–	–	26
$CuO/ZnO/Al_2O_3$	1	227	>0.33	24	1.1	0	28
$CuO/ZnO/Al_2O_3$	1	227	<0.33	24	0.3	0.8	28
Pt/YSZ (open circuit)	1	650–800	0.2–2	15.6	0.7	0.53	This work
Pt/YSZ (−1000 mV)	1	650–800	0.2–2	5.4	0.75	0.12	This work
Pt/YSZ (400 mV)	1	650–800	0.2–2	6.9	0.47	0.42	This work

It should be underlined here that electrocatalytic apparent activation energies were similar whether a positive or a negative voltage is imposed to the cell. This similar decrease in apparent activation energies indicates, that either a different but common reaction step, other than the one in the pure catalytic process, determines the reaction rate or, by applying the electrochemical promotion technique, the rate determining step is facilitated and consequently the activation barrier is substantially decreased. As far as the CO_2 and H_2 conversions concerning both experimental conversions were much lower than those predicted by thermodynamics (58.8% at 650 °C to 70.6% at 800 °C) and consequently kinetics, rather than thermodynamics, controls the whole process.

As discussed below, this obvious enhancement (10-fold rate increase) in the CO formation reaction rate (Fig. 1) can be explained using the electrochemical promotion theory, developed by Vayenas et al. [33]. It is well known, that applying a certain voltage on the catalyst–electrode leads to a corresponding change in its work function, which is responsible for the observed electrochemical promotion phenomenon and can be directly related with the enhancement of CO_2 and H_2 adsorption. The effect of EP can be attributed to the electrochemically induced and controlled migration of ions, from the solid electrolyte onto the gas-exposed electrode surface which affects the catalytic phenomena taking place there, in a very pronounced, reversible and controlled manner [33]. Therefore, by imposing positive voltages, the electrode-catalyst is positively charged, while at negative potentials the electrode is reduced and is negatively charged (due to an excess of electrons).

Fig. 2 presents the effect of CO_2 partial pressure on the CO formation rate and cell electromotive force (EMF) at constant P_{H_2}, equal to 5 kPa and at temperature of 725 °C. Rate increases with increasing P_{CO_2} at both open and closed circuit operation, indicating a clear positive effect on the reaction rate. Also in the present case, it was observed that at negative voltages, CO formation rate was significantly increased, while at positive voltages it was decreased, however to a less extent.

In Fig. 2b the effect of CO_2 partial pressure on the developed open circuit potential is depicted. The electromotive force increases with CO_2 partial pressure and therefore with CO_2 coverage, indicating that carbon dioxide acts as a pure acceptor of electrons that are derived from the electrode surface. Therefore, CO_2 prefers to be adsorbed on surfaces that are capable to provide electrons in order to form the chemisorptive bond, thus increasing CO_2 coverage on the catalyst–electrode surface. By forming the adsorbate-electrode bond, the intra-adsorbate bonds are weakened, favouring also to some extent the dissociation of the adsorbate. In general, EMF performance could be interpreted on the basis of the Nernst's equation, which shows that by increasing oxygen activity (not always gas phase concentration) on the anodic electrode, the corresponding electromotive force increases.

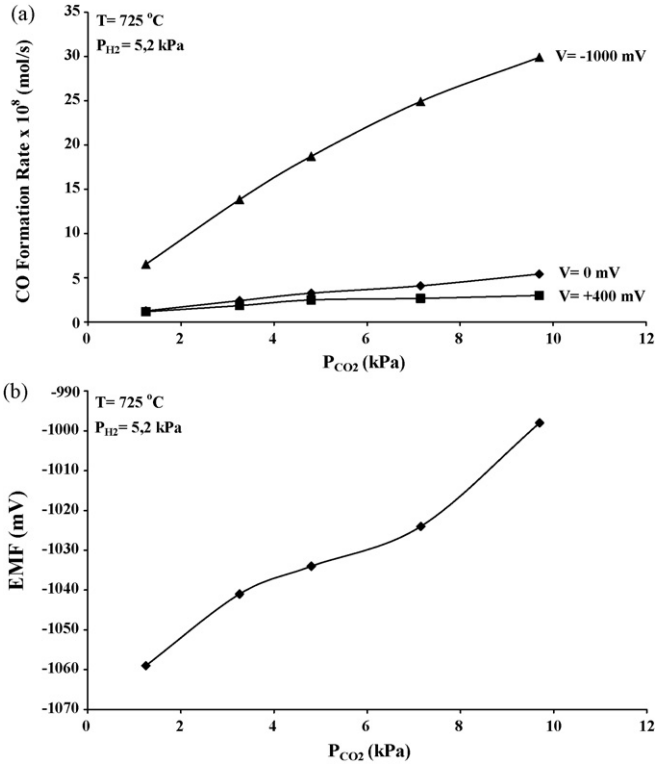

Fig. 2. Effect of CO_2 partial pressure on (a) CO formation rate under open (0 mV) and closed (−1000 and 400 mV) circuit operation and (b) electromotive force of the cell. $T = 725$ °C, $P_{H_2} = 5.2$ kPa, $P_{CO_2} = 1-10$ kPa, $F_T = 20$ cm^3/min.

The corresponding apparent CO_2 reaction order under open circuit conditions was equal to 0.7. During cathodic operation, CO_2 apparent reaction order was more or less similar with the open circuit value (0.75), implying the participation of the same fractional intermediate in both cases, but higher than the corresponding value at anodic conditions (0.47). It is interesting to note that at higher positive potentials, the corresponding reaction order exhibits a tendency to reach zero. The apparent reaction order indicates the extent in which a reactant molecule participates in the rate-determining step. Therefore, it can be concluded that favouring H_2 adsorption, CO_2 adsorption is inhibited and thus, cannot participate in the reaction. Consequently, at high positive potentials the dominate reaction is the (electro-)oxidation of H_2.

In Fig. 3, the dependence of CO formation rate (Fig. 3a) and open circuit potential (Fig. 3b) on the hydrogen partial pressure at $P_{CO_2} = 5$ kPa and $T = 725$ °C, is shown. As far as the CO formation rate concerns, qualitatively similar results were obtained with the case of Fig. 2a, e.g. CO formation rate increases with increasing hydrogen partial pressure, while the same effect was observed in the case of closed circuit operation. However, the dependence of EMF on the hydrogen partial pressure is different when compared to the previous case. EMF decreases with increasing P_{H_2}, implying that H_2 acts as an electron donor, indicating that by decreasing catalyst's work function, hydrogen coverage increases. In contrary to the case of CO_2, hydrogen is strongly attracted by positively charged surfaces. Such a case is, at positive potentials, when oxygen anions are transported from cathode to anode.

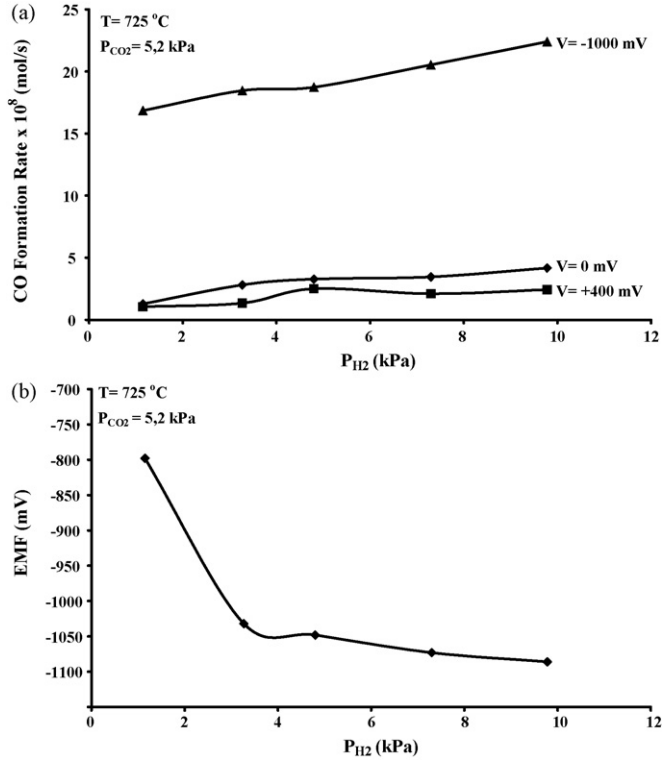

Fig. 3. Effect of H_2 partial pressure on (a) CO formation rate under open (0 mV) and closed (−1000 and 400 mV) circuit operation and (b) electromotive force of the cell. $T = 725$ °C, $P_{H_2} = 1-10$ kPa, $P_{CO_2} = 5.2$ kPa, $F_T = 20$ cm^3/min.

Hydrogen reaction order is also positive, but lower, compared to the corresponding CO_2 reaction order and equals to 0.53, indicating that probably hydrogen ad-atoms are participating in the rate determining step. Under closed circuit operation conditions, the corresponding reaction orders were different. Specifically, at positive potentials, the calculated H_2 reaction order was close to that of the open circuit (hydrogen ad-atoms are participating in the rate determining step), while tended to zero in the case of negative potentials.

As it was stated before, the open circuit kinetics (Table 1) were positive order in both the electron acceptor and electron donor reactant. In the context of Langmuir–Hinshelwood type kinetics, this means that both reactants are weakly adsorbed (low adsorption constants—low CO_2 and H_2 coverages) on the catalyst surface. As it was referred in Section 1, where both the redox and the associative formate mechanisms are described, the first mechanism is strongly based on the catalysts' support which under consecutive redox cycles is contributing to the formation of CO and H_2O in the RWGS reaction. Therefore, the redox mechanism requires the existence of an appropriate support that would have the capability to be consecutively oxidized and reduced. In the present case, there is not such a support and it must be noticed that under the employed reaction conditions platinum is impossible to be oxidized and its reduced form (metallic platinum) prevails the electrode's surface. Therefore, even though no surface characterization measurements (e.g. FTIR, DRIFTS, XPS, etc.) were performed in order to support the hypothesis of formate intermediate formation, it can be assumed based on the related literature [34] and on kinetic data that catalytic RWGS reaction follows the formate decomposition mechanism, which can be represented by the following equations:

$$CO_2 + Pt \leftrightarrow CO_{2,ad} \quad (2)$$

$$H_2 + 2Pt \leftrightarrow 2H_{ad} \quad (3)$$

$$CO_{2,ad} \leftrightarrow C_{inter} \quad (4)$$

$$C_{inter} + H_{ad} \leftrightarrow [HCOO] \leftrightarrow CO_{ad} + OH_{ad} \quad (5)$$

$$CO_{ad} \leftrightarrow CO + Pt \quad (6)$$

$$OH_{ad} + H_{ad} \leftrightarrow H_2O + 2Pt \quad (7)$$

Step (2) reflects the fast, molecular associative, weak adsorption of CO_2 on a Pt-site, while step (3) represents hydrogen dissociative adsorption on two Pt active centers. Following that, in step (4), a specific C-containing intermediate is formed, which can interact with adsorbed hydrogen, producing oxy-hydrogenated carbonylic intermediate species, subsequently decomposing to adsorbed CO and hydroxyls (step 5). Steps (6) and (7) complete the reaction mechanistic scheme and are associated with CO desorption and water formation. By taking into account the fractional CO_2 apparent reaction order and the corresponding half reaction order of hydrogen, it seems that most probably, steps (4) and (5) are controlling the RWGS reaction rate.

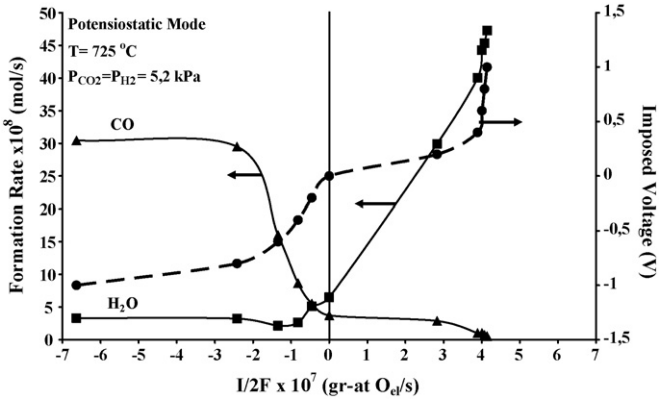

Fig. 4. Dependence of CO and H_2O formation rate on the electrochemical oxygen supply/removal rate and cell imposed voltage. $T = 725\ ^\circ C$, $P_{H_2} = P_{CO_2} = 5.2$ kPa, $F_T = 20\ cm^3/min$.

Fig. 4 shows the effect of electrochemical oxygen supply/removal on the CO and H_2O formation rates at stoichiometric reactants' ratio and at 725 °C, under potentiostatic mode of operation. It is clear that CO formation rate is dramatically enhanced at negative potentials reaching a plateau at voltages higher than −800 mV, while it decreases to a less extent at positive potentials. The opposite behaviour was observed in the case of H_2O formation rate which was slightly decreased at negative potentials reaching a plateau at voltages higher than −400 mV and increased almost linearly at positive potentials. An interesting remark is that water formation rate was increased as the voltage increased. However, it can be seen that at potentials higher than 400 mV a limiting current was achieved, which can be attributed to mass transport limitations. It must be noticed here that limiting currents are observed under mass transport or diffusion limitations of charge and/or neutral chemical species. By taking into account that hydrogen conversion at positive potentials is higher than approximately 50% and CO has been essentially eliminated at potentials higher than 400 mV, it can be considered that mass transport limitations are determining the whole process, since oxygen anions cannot oxidize either CO (it has been already disappeared) or hydrogen, which due to its high conversion is difficult to reach the electrode/catalyst surface. On the contrary, in the case of cathodic polarization conditions, oxygen anions are transferred from anode (CO_2, CO and H_2O are the oxygen containing compounds) to cathode and the corresponding conversion of CO_2 is not as much higher as in the case of the corresponding hydrogen conversion at anodic polarization. Therefore, there are no mass transport limitation problems and this is the reason why limiting currents are not observed under cathodic polarization conditions.

This impressive enhancement in CO and H_2O formation rates was attributed to EP and the phenomenon was non-Faradaic. Many times in the past, it was found that this promotional effect of various catalytic reactions was non-Faradaic, as in the case of the RWGS reaction studied over Rh and Pd [33,34]. Vayenas and co-workers defined the rate enhancement factor, Λ, as [33]:

$$|\Lambda| = \frac{|\Delta r|}{|I/2F|} \tag{8}$$

where $|\Delta r|$ is the absolute increase in the catalytic CO and H_2O formation rates (expressed in gr-atoms of oxygen per second) and $|I/2F|$ is the imposed flux of O^{2-} through the electrolyte (also expressed in gr-atoms of oxygen per second). In the case of a Faradaic effect, the enhancement factor $|\Lambda|$ equals to unity, while $|\Lambda|$ values exceeds unity in the case of non-Faradaic operation [33].

Fig. 5 depicts the effect of electrochemical oxygen supply/removal rate on the Δr of CO and H_2O formation. Differently dashed lines represent $|\Lambda|$ values equal to 10 and unity, respectively. It seems that a non-Faradaic behavior ($|\Lambda| = 10$) stands for the cases of CO formation at negative currents and water formation at positive currents, while in the opposite cases $|\Lambda|$ was decreased and tended to unity, e.g. to purely Faradaic operation. This difference implies that at high $|\Lambda|$ values direct electrocatalysis, together with the electrochemical promotion, determine the RWGS reaction, while at $|\Lambda| = 1$, RWGS reaction shifts clearly to either CO_2 and H_2O (electro)-decomposition (at negative potentials) or to H_2 and CO (electro-)oxidation (at positive potentials).

Vayenas et al., in their comprehensive analysis on the electrochemical activation of catalysis [33], developed some simple rules predicting the behaviour of reactions under electrochemical promotion. It was stated among the others, that a reaction exhibits inverted volcano (minimum rate) type behaviour versus the applied potential when the kinetics are positive order in both the electron acceptor (CO_2) and electron donor (H_2) reactants. This was not observed in our experiments, since as shown in Fig. 4, CO formation rate was increased as voltage was decreased (purely electrophobic behavior), while water formation rate was increased by increasing catalyst potential (purely electrophilic behavior). Therefore, RWGS reaction is converted to the corresponding monomolecular reactions stated in the previous paragraph, justifying the obtained lower reaction orders for CO_2 and H_2, with respect to

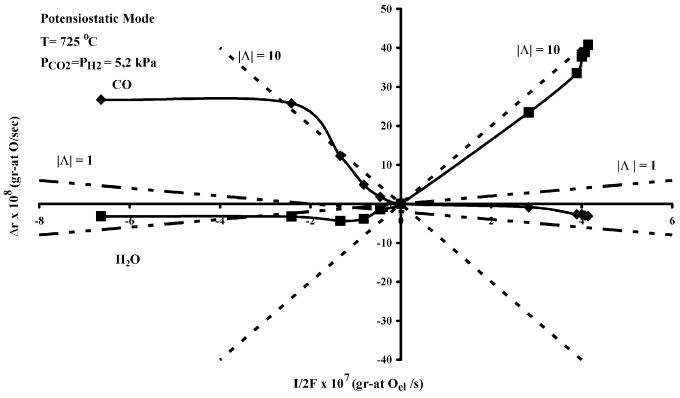

Fig. 5. Effect of electrochemical oxygen supply/removal rate on the change of the catalytic rate, Δr. $T = 725\ ^\circ C$, $P_{H_2} = P_{CO_2} = 5.2$ kPa, $F_T = 20\ cm^3/min$.

the corresponding open circuit values, in the case of high positive and negative potentials, respectively.

By applying negative potentials, F-centers are formed, either on the three phase boundary between electrode, solid electrolyte and gas phase or at the interfaces of gas phase-solid electrolyte or electrode-solid electrolyte and in the following CO_2 and H_2O are decomposed to CO, H_2 and lattice oxygen in YSZ:

$$V_o^{\bullet\bullet}(s) \leftrightarrow V_o^x(s) + 2h_{electrode}^{\bullet} \quad (9)$$

where $V_o^{\bullet\bullet}(s)$, is an oxygen vacancy on the solid electrolyte surface, $V_o^x(s)$ is an F-center (neutral oxygen vacancy) and $h_{electrode}^{\bullet}$ is an electron hole (deficits of electronegativity), transferred from the electrolyte to the electrode. In the following, these F-centers can directly decompose CO_2 and H_2O:

$$CO_2 + V_o^x(s) \leftrightarrow CO + O_o^x(s) \quad (10)$$

$$H_2O + V_o^x(s) \leftrightarrow H_2 + O_o^x(s) \quad (11)$$

where $O_o^x(s)$, is a lattice oxygen on the YSZ surface, which will be introduced in the YSZ lattice structure:

$$O_o^x(s) + V_o^{\bullet\bullet}(b) \leftrightarrow V_o^{\bullet\bullet}(s) + O_o^x(b) \quad (12)$$

where (s) denotes the surface of the electrolyte and (b) the bulk of the electrolyte.

It must be mentioned here, that if CO_2 and H_2O react at sites different than F-centers, then the gas species can be transported either by spillover on the electrode surface or via bulk diffusion through the electrode mass, towards F-centers to react electrochemically [Eqs. (10) and (11)]. However, as we observed in Fig. 4, over −600 mV only CO_2 reacted, while H_2O remained unaffected. This observation can be attributed to the limited amount of water present in the reactor, as well as to the increased capability of CO_2 to diffuse more easily than water over and through the electrode. Finally, at very high voltages (more than −800 mV) CO formation reaction rate was stable, implying either CO_2 diffusion limitation problems or limited available F-centers.

On the other hand, at positive voltages, lattice oxygen anions are formed at F-centers, which can directly react with hydrogen or CO to produce water and CO_2, respectively. It was clearly shown that CO was oxidized until it was diminished, while water formation rate was dramatically enhanced by increasing catalyst potential. Finally, at higher voltages, limiting currents were observed due to mass transfer limitations.

However, Λ values up to 10 were achieved, indicating that not only direct electrocatalysis but also the enhancement of the pure catalytic rate contribute to the promoted observed rates. It can be proposed that a similar reaction mechanism stands also for the case of closed circuit operation and that these changes in the catalyst–electrode work function are responsible for the decrease in the activation energy and therefore for the promotion of the reaction rate.

Consequently, at anodic polarization conditions, where hydrogen coverage is enhanced and water formation is linearly increased, the formation of an electron donor oxy-hydrogenated carbonylic intermediate is strongly promoted, facilitating H_2O formation. The mechanism starts with reactions (2)–(4) [reaction (3) is carried out twice], followed by the interaction of a C-containing intermediate with a hydrogen and a mobile oxygen anion ad-atoms. The intermediate is reduced, thus forming a negative oxy-hydrogenated carbonylic species. This intermediate species is then decomposed to carbon monoxide and other species and supplies two electrons (as an electron donor) back to the electrode:

$$C_{inter} + H_{ad} + {O_{ad}}^{2-} \leftrightarrow [HCOO]^{2-} + O_{ad} \leftrightarrow CO_{ad} + OH_{ad} + O_{ad} + 2e- \quad (13)$$

In the following, OH_{ad} and O_{ad} species together with two more hydrogen ad-atoms (a reminder that at positive voltages hydrogen coverage is much higher than CO_2 coverage) interact, producing two molecules of water.

$$O_{ad} + H_{ad} \leftrightarrow OH_{ad} + Pt \quad (14)$$

$$2x(OH_{ad} + H_{ad} \leftrightarrow H_2O + 2Pt) \quad (15)$$

The reaction is completed with step (6). It must be noticed here, that the Pt-site in Eq. (14) was originated by the oxygen anion ad-atom coming from the YSZ lattice structure. The above mechanism is in accordance with our experimental observations, explaining the positive reaction orders of the reactants, as well as the lower activation energy calculated at positive potentials.

On the other hand, at negative voltages the following mechanistic scheme can be employed to describe the RWGS reaction rate:

$$2x(CO_2 + Pt \leftrightarrow CO_{2,ad}) \quad (2')$$

$$H_2 + 2Pt \leftrightarrow 2H_{ad} \quad (3')$$

$$2x(CO_{2,ad} \leftrightarrow C_{inter}) \quad (4')$$

$$C_{inter} + H_{ad} \leftrightarrow [HCOO] \leftrightarrow [HCO]^{2+} + {O_{ad}}^{2-} \quad (16)$$

$$C_{inter} + [HCO]^{2+} + 2e^- \leftrightarrow 2CO_{ad} + OH_{ad} \quad (17)$$

$$2x(CO_{ad} \leftrightarrow CO + Pt) \quad (6')$$

$$OH_{ad} + H_{ad} \leftrightarrow H_2O + 2Pt \quad (7')$$

In detail, reaction starts with the associative adsorption of two molecules of CO_2 and the dissociative adsorption of hydrogen (CO_2 coverage is higher at cathodic operation conditions, compared to the corresponding hydrogen coverage). In the following, the first C-containing intermediate interacts with a hydrogen ad-atom and forms an oxy-hydrogenated species, which is decomposed to a positive charged species and an oxygen anion ad-atom, ${O_{ad}}^{2-}$, afterwards directed towards the YSZ lattice structure. This species reacts with the second C-containing intermediate and two electrons (as an electron acceptor) and decomposes to OH_{ad} and two adsorbed CO molecules. Finally, reactions (6) and (7) complete the sequence of reaction steps. Additionally, in the case of imposing negative voltages to the cell, the formation and decomposition of an electron acceptor oxy-hydrogenated

carbonylic intermediate is strongly promoted, enhancing the production of CO.

However, from the above mechanistic schemes it seems, that CO (at anodic operation) and water (at cathodic operation) are also formed, while in Fig. 4 it was observed that both rates are decreased at low voltages. This difference can be attributed to CO direct (electro-)oxidation (at positive potentials) and H_2O direct (electro-)decomposition (at negative potentials) that are proceeding very fast, as compared with the above reaction mechanisms.

In conclusion, all proposed mechanisms under open and closed circuit operation are based on the associative formate formation and decomposition mechanism. At anodic polarization conditions, hydrogen (electron donor) adsorption is enhanced as long as the applied potential increases and consequently hydrogen coverage is always higher compared to the corresponding coverage of CO_2 resulting to the enhanced water formation through the direct (electro-)oxidation of hydrogen. On the other hand, at cathodic potentials CO_2 as an electron acceptor is prevailing on the electrode's surface and as a consequence the formation of CO through the direct (electro-)decomposition of CO_2, is enhanced especially at high cathodic voltages. Therefore, by taking into account the above aspects, the observed differences in CO_2 and H_2 reaction orders under open and closed (anodic and cathodic polarization) circuit kinetics, can be explained.

Moreover, from the previous analysis of the proposed mechanisms, it seems that the formation and decomposition of the formate intermediate species plays a crucial role in the overall mechanism. At anodic potentials the formation of the electron donor formate intermediate, i.e. $[HCOO]^{2-}$, is enhanced and then is decomposed by simultaneously deliberating electrons. On the contrary, at cathodic potentials the decomposition of the formate intermediate is enhanced leading initially to an electron acceptor species, i.e. $[HCO]^{2+}$, which is further dissociated to the final products.

Finally, an interesting remark is that the observed NEMCA behaviour does not follow the rules of electrochemical promotion [33], an observation which can be attributed to the fact that the RWGS reaction is shifted to the corresponding monomolecular reactions, i.e. CO_2 and H_2O (electro-)decomposition at negative voltages and CO and H_2 (electro-)oxidation at positive ones.

3.2. "RWGS" SOFC operation

As previously suggested in the introduction section, it was very interesting to explore the potential role of the RWGS reaction in the production of "green" electrical energy in a SOFC, considering that mixtures of CO_2 and H_2 are produced during biomass thermochemical conversion (e.g. gasification, pyrolysis). Therefore, the effect of cell temperature and P_{CO_2}/P_{H_2} ratio on the voltage–current density and power density–current density characteristics was investigated.

Fig. 6a shows the effect of cell temperature (700–800 °C) on voltage–current and power output–current data at a stoichiometric ratio of reactants ($P_{H_2} = P_{CO_2} = 5$ kPa). The results

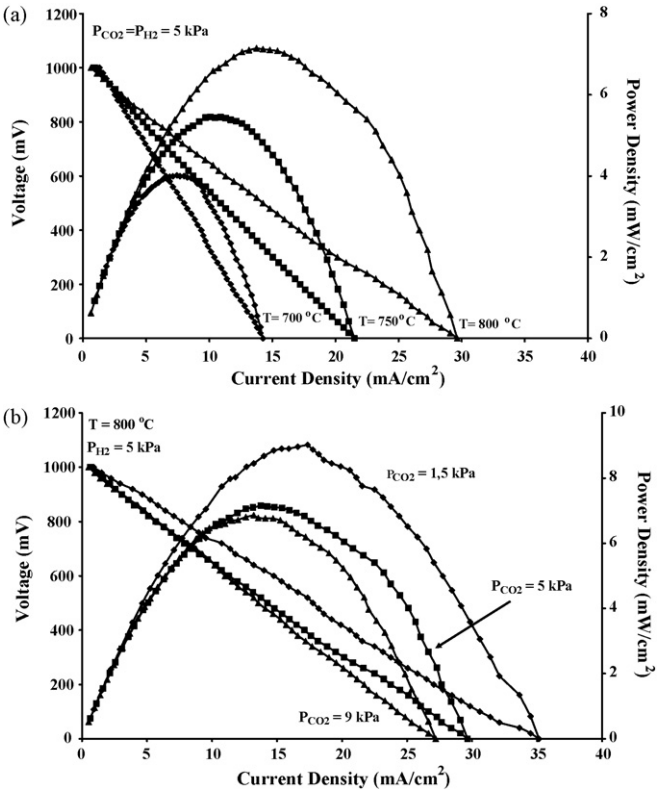

Fig. 6. Current density–voltage and current density–power density characteristics of the SOFC. (a) Effect of cell temperature and (b) effect of P_{CO_2}/P_{H_2} ratio. T = 700–800 °C, P_{H_2} = 5 kPa, P_{CO_2} = 1.5–9 kPa, F_T = 20 cm^3/min.

show a clear, linear dependence of cell voltage on current density, which demonstrates the predominant contribution of the extremely high ohmic resistance on the overall cell polarization in comparison to activation and concentration polarizations. The slopes of the voltage–current curves determine the ohmic resistance of the cell, a significant part of which is due to the O^{2-} transport resistance of the thick (1–2 mm) YSZ solid electrolyte. In order to quantify the partial contribution of the different types of polarization to the overall resistance, impedance data is needed. Since there are no such data available, is difficult to conclude how the anodic and cathodic charge transfer reactions (activation overpotential), employed over the whole temperature range and moreover how mass transfer or diffusion limitations (concentration overpotential) involving the electrode pores are participating in the overall fuel cell performance. However, the linear *V–I* dependence clearly indicates the absence of activation and concentration overpotentials under the employed operating conditions. Concerning current density–power density characteristics it is clear that the achieved power density increases as temperature increases, where ohmic resistances are obviously decreasing. A 70% increase in power generation was achieved by increasing cell temperature from 700 to 800 °C. A maximum power output of 7 mW/cm^2 was obtained at a cell voltage of 520 mV and a current density of 13.75 mA/cm^2, at 800 °C.

Fig. 6b presents typical voltage–current density and power density–current density closed circuit data of the RWGS-SOFC

operating at three different P_{CO_2}/P_{H_2} molar feed ratios. Since one of the principal limitations of biogas is its variability of quality (H_2 content), attention was given to the capability of the present fuel cell to satisfactorily operate under poor quality fuel feed. Therefore, the effect of P_{CO_2} (1.5–9 kPa) on the production of power output at constant P_{H_2} equal to 5 kPa and at $T = 800\ ^\circ C$ was examined. Once more, only the ohmic polarization was noticed, while activation and concentration polarizations were absent under these reaction conditions. It was observed that the produced electrical energy was increased as the P_{CO_2}/P_{H_2} ratio was decreasing, implying that the efficiency of the ''RWGS'' SOFC is strongly related to the hydrogen content of the feeding fuel. This observation is in accordance with the (electro-)kinetic studies on the RWGS reaction, showing that at Pt-polarized (positive potentials) surfaces hydrogen, as an electron donor, is (electro-)oxidized much faster than CO. This fact is related with the difference in the concentrations of hydrogen and CO and moreover with diffusion limitations, since hydrogen is a much more mobile molecule than CO. Under these reaction conditions, a maximum power output (9 mW/cm^2) was achieved at 520 mV cell voltage and a current density of 17.35 mA/cm^2, at 800 °C. The low maximum power output observed in the present work in comparison to other related literature results [37] can be attributed mainly to the lower concentrations of the employed fuels fed (H_2) or produced internally (CO) in the SOFC and to low operating temperatures, compared to other literature works. Moreover, the thickness of the YSZ reactor was approximately 2 mm, which constitutes an important obstacle in order to achieve high power outputs. Finally, in lab experiments it is difficult to set up an effective current collector configuration (i.e. use of state of the art interconnectors) and usually significant power losses are revealed in such systems. Therefore, substantial improvements in power generation could be obtained by using state of the art anodic composites, thinner YSZ components, better interconnectors or working at elevated temperatures and higher fuels concentrations. It must be noticed here that at very high P_{CO_2}/P_{H_2} ratios the generated energy was disproportionally low and at several times it was impossible to obtain stable measurements, probably due to carbon deposition.

Finally, long-term operation experiments, for more than 12 h time on stream, at stoichiometric reactants' ratio ($P_{H_2} = P_{CO_2} = 5$ kPa) and at 800 °C were performed. These experiments demonstrated that the ''RWGS'' SOFC exhibited a very stable behavior and can be considered as a promising alternative route for the production of ''green'' power from biomass, since CO_2 and H_2 gas mixtures are the main products of biomass thermochemical conversion processes.

4. Conclusions

In the present work, the (electro-)kinetics of the RWGS reaction were studied in a SOFC of the type Pt/YSZ/Pt. The effect of imposed potentials, cell temperature, H_2 and CO_2 partial pressures on the kinetics and mechanism of the catalytic and electrocatalytic RWGS reaction, was systematically examined. The apparent catalytic activation energy was found equal to 15.6 kcal/mol, while H_2 and CO_2 apparent reaction orders were equalled to 0.5 and 0.7, respectively. Under open circuit operation, the formate decomposition reaction mechanism was considered to describe kinetics. The formation of a C-containing intermediate and its interaction with atomically adsorbed hydrogen to form oxy-hydrogenated carbonylic species, which subsequently decompose to CO and hydroxyls, seems to control the RWGS reaction rate.

Under closed circuit operation, direct electrocatalysis (electro-decomposition of CO_2 and H_2O at negative potentials and electro-oxidation of CO and H_2 at positive potentials) together with the enhancement of the open circuit reaction rate (Λ values up to 10 were achieved) explain the enhanced CO (at negative voltages) and H_2O (at positive potentials) formation rates. Therefore, this dramatic increase observed in the CO and H_2O formation rates was attributed both to the electrocatalytic oxidation or decomposition as well as to the enhancement of the catalytic reaction rate, through the promoted formation of the electron donor (at positive potentials) and decomposition of the electron acceptor (at negative potentials) oxy-hydrogenated carbonylic intermediates.

Finally, current density–voltage and current density–power density characteristics of the cell were measured at various temperatures and mixtures of CO_2 and H_2. It was found that in all cases the amount of produced electricity was maximized by increasing cell temperature and decreasing CO_2/H_2 feed ratio. Ohmic polarization dominated the overall cell polarization, implying its main contribution due to the high ohmic resistance in comparison to the activation and concentration polarizations. Long-term operation experiments demonstrated that the RWGS SOFC exhibited great stability and durability and can be considered as an alternative route for the production of ''green'' power from biomass conversion processes.

Acknowledgements

The authors would like to acknowledge financial support from the Greek Ministry of National Education and Religious Affairs through the framework of PYTHAGORAS research program.

References

[1] M.A. Pena, J.P. Gomez, J.L.G. Fierro, Appl. Catal. A: Gen. 144 (1–2) (1996) 7–57.
[2] S. Freni, G. Calogero, S. Cavallaro, J. Power Sources 87 (1/2) (2000) 28–38.
[3] T. Osaki, N. Narita, T. Horiuchi, T. Sugiyama, H. Masuda, K. Suzuki, J. Mol. Catal. A 125 (1997) 63–71.
[4] J.T.S. Irvine, A. Sauvet, Fuel Cells 1 (3–4) (2001) 205–210.
[5] A.V. Bridgwater, Chem. Eng. J. 91 (2003) 87–102.
[6] P. McKendry, Bioresource Technol. 83 (2002) 55–63.
[7] G. Avgouropoulos, J. Papavasiliou, T. Tabakova, V. Idakiev, T. Ioannides, Chem. Eng. J. 124 (2006) 41–45.
[8] C. Song, Catal. Today 115 (1–4) (2006) 2–32.
[9] A. Goguet, S.O. Shekhtman, R. Burch, C. Hardacre, F.C. Meunier, G.S. Yablonsky, J. Catal. 237 (2006) 102–110.

[10] G. Wang, L. Jiang, Y. Zhou, Z. Cai, Y. Pan, X. Zhao, Y. Li, Y. Sun, B. Zhong, X. Pang, W. Huang, K. Xie, J. Mol. Struct. (Theochem.) 634 (1–3) (2003) 23–30.
[11] T. Bunluesin, R.J. Gorte, G.W. Raham, Appl. Catal. B: Environ. 15 (1998) 107–114.
[12] S. Hilaire, X. Wang, T. Luo, R.J. Gorte, J. Wagner, Appl. Catal. A: Gen. 215 (2001) 271–278.
[13] T. Bunluesin, R.J. Gorte, G.W. Raham, Appl. Catal. B: Environ. 14 (1997) 105–115.
[14] H. Cordatos, T. Bunluesin, J.S. Stubenrauch, J.M. Vohs, R.J. Gorte, J. Phys. Chem. 100 (1996) 785–789.
[15] R.J. Gorte, S. Zhao, Catal. Today 104 (2005) 18–24.
[16] T. Shido, Y. Iwasawa, J. Catal. 141 (1993) 71–81.
[17] G. Jacobs, L. Williams, U. Graham, D. Sparks, B.H. Davis, J. Phys. Chem. B 107 (2003) 10398–10404.
[18] G. Jacobs, E. Chenu, P.M. Patterson, L. Williams, D. Sparks, G. Thomas, B.H. Davis, Appl. Catal. A: Gen. 258 (2004) 203–214.
[19] G. Jacobs, B.H. Davis, Appl. Catal. A: Gen. 284 (2005) 31–38.
[20] G. Jacobs, A.C. Crawford, B.H. Davis, Catal. Lett. 100 (2005) 147–152.
[21] G. Jacobs, U.M. Graham, E. Chenu, P.M. Patterson, A. Dozier, B.H. Davis, J. Catal. 229 (2005) 499–512.
[22] G. Jacobs, P.A. Patterson, U.M. Graham, D.E. Sparks, B.H. Davis, Appl. Catal. A: Gen. 269 (2004) 63–73.
[23] C.R. Prichard, N.J. Hinshelwood, J. Chem. Soc. 127 (1925) 806–810.
[24] Y. Amenomiya, J. Catal. 55 (2) (1978) 205–212.
[25] Y. Amenomiya, J. Catal. 57 (1) (1979) 64–71.
[26] J. Yoshihara, C.T. Campbell, J. Catal. 161 (1996) 776–782.
[27] A.B. Mhadeshwar, D.G. Vlachos, Catal. Today 105 (2005) 162–172.
[28] M.J.L. Gines, A.J. Marchi, C.R. Apesteguia, Appl. Catal. A: Gen. 154 (1997) 155–171.
[29] C.-S. Chen, W.-H. Cheng, S.-S. Lin, Appl. Catal. A: Gen. 257 (2004) 97–106.
[30] A. Goguet, F. Meunier, J.P. Breen, R. Burch, M.I. Petch, A.F. Ghenciu, J. Catal. 226 (2004) 382–392.
[31] S. Pancharatnam, R.A. Huggins, D.M. Mason, J. Electrochem. Soc. 122 (7) (1975) 869–875.
[32] M. Stoukides, Catal. Rev. Sci. Eng. 42 (2000) 1–70.
[33] C.G. Vayenas, S. Bebelis, C. Pliangos, S. Brosda, D. Tsiplakides, Electrochemical Activation of Catalysis, Kluwer Academic/Plenum Publishers, New York, 2001.
[34] H. Karasali, Ph.D. Thesis, Department of Chemical Engineering, University of Patras, 1988.
[35] G. Karagiannakis, S. Zisekas, M. Stoukides, Solid State Ionics 162–163 (2003) 313–318.
[36] G. Marnellos, S. Zisekas, A. Kungolos, Appl. Catal. B: Environ. 42 (3) (2003) 225–236.
[37] R.J. Gorte, J.M. Vohs, S. McIntosh, Solid State Ionics 175 (2004) 1–6.